Surface-Charge-Switchable Nanoclusters for Magnetic Resonance Imaging-Guided and Glutathione Depletion-Enhanced Photodynamic Therapy

Jianzhi Zhu[1,2#], Tingting Xiao[2#], Jiulong Zhang[3], Hailong Che[1], Yuxin Shi[3], Xiangyang Shi[2*] and Jan C. M. Hest[1*]

1 Bio-Organic Chemistry, Institute for Complex Molecular Systems, Eindhoven University of Technology, 5600 MB Eindhoven, the Netherlands

2 State Key Laboratory for Modification of Chemical Fibers and Polymer Materials, International Joint Laboratory for Advanced Fiber and Low-dimension Materials, College of Chemistry, Chemical Engineering and Biotechnology, Donghua University, Shanghai 201620, People's Republic of China

3 Department of Radiology, Shanghai Public Health Clinical Center, Fudan University, Shanghai 201508, People's Republic of China

Materials

All materials were purchased from Sigma-Aldrich unless otherwise noted. Dulbecco's modified eagle's medium (DMEM), trypsin, penicillin/streptomycin (P/S), fetal bovine serum (FBS), phosphate-buffered saline (PBS), Hoechst 33342, MitoTracker™ Red CMXRos, LysoTracker™ Green DND-26 and singlet oxygen sensor green (SOSG) were purchased from ThermoFisher Scientific. Chlorin e6 (Ce6) was acquired from Frontier Scientific, Inc. Glycol chitosan (GC) was purchased from Santa Cruz Biotechnology, Inc. All chemicals and materials were used without further purification.

Instruments

Malvern Z90 Zetasizer equipped with a 633 nm laser and an avalanche photodiode detector was employed to characterize the hydrodynamic size and zeta potential. ^{1}H NMR spectra were obtained on a Bruker 400 NMR spectrometer. Transmission Electron Microscopy (TEM) images were captured on a FEI Tecnai 20 (type Sphera). Scanning electron microscopy (SEM) images were recorded by FEI Quanta 200 3D FEG. The particle size distribution was measured using Image J software with counting at least 200 particles randomly selected from TEM or SEM images. The fluorescence spectra were acquired using a PerkinElmer LS55 fluorescence spectrometer at 293 K, with 2.5 nm slit width and excitation wavelength of 400 nm. Confocal laser scanning microscopy (CLSM) images were observed on a Leica TCS SP5X. A flow cytometer (BD Biosciences, USA) was used to quantify the cellular uptake amount and the data was analyzed using FlowJo software. Ultraviolet–visible Spectroscopy (UV/Vis) absorbance was recorded on a Jasco V-650 UV/Vis spectrometer. XPS spectra were obtained on a Thermo Scientific K-Alpha spectrometer. The O_2 concentration was measured with a portable meter MultiLine® Multi 3510 IDS. MTT absorbance was recorded with a microplate reader (Safire2, TECAN). Mn concentration was measured with inductively coupled plasma-optical emission spectroscopy (ICP-OES, Leeman Prodigy).

Cell Culture

Human embryonic kidney cells 293 (HEK 293), mice embryonic fibroblast cells (NIH 3T3) and HeLa cells were cultured in DMEM supplemented with 10% FBS and 1% P/S at 37 ^{o}C, 5% CO_2 and 70% humidity. To prepare DMEM with an acidic pH of 6.5, 1 M HCl was used to adjust the medium pH to 6.5, and the medium was filtered with a sterile filter (pore size 0.2 μm) for immediate use.

Cell Viability Assays

Dark cytotoxicity of Ce6, GCC, BMGCC and CMGCC towards HEK 293 cel ls at pH 7.4 and HeLa cells at pH 7.4 and 6.5 were evaluated using standard MTT. Briefly, cells were seeded in a 96-well plate at a density of 5 000 cells/well and cultured overnight. The medium was removed and the cells were further treated with fresh medium containing free Ce6, GCC, BMGCC or CMGCC at the same Ce6 concentrations (0, 0.25, 0.5, 1, 2, 3, 4 and 5 μg/mL) and cultured for another 24 h. The medium was removed carefully, and the cells were incubated with 100 μL of DMSO supplemented with 10% MTT for 4 h. The absorbance at 540 nm was recorded on the microplate reader. For

each sample concentration, 6 parallel experiments were analyzed to give a mean value and standard deviation.

To investigate the cell viability upon laser irradiation, HeLa cells were seeded in a 96-well plate at a density of 5 000 cells/well and cultured overnight. The cells were further incubated with medium containing free Ce6, GCC, BMGCC or CMGCC at the same Ce6 concentrations (0, 0.25, 0.5, 1, 2, 3, 4 and 5 μg/mL) at physiological pH of 7.4 and tumor microenvironment pH of 6.5 for 4 h before laser irradiation (660 nm, 100 mW/cm^2, 5 min). The cells were further cultured for 20 h and the cytotoxicity was then measured following the same procedure mentioned above.

To visualize the PDT-induced cytotoxicity with fluorescent staining, HeLa cells were incubated with free Ce6, GCC, BMGCC or CMGCC ([Ce6] = 0.5 μg/mL) at pH 7.4 or 6.5 for 4 h, followed by laser irradiation for 5 min (100 mW/cm^2). After culturing for 8 h, the cells were stained with Hoechst, FITC-Annexin V and PI, and observed under CLSM.

***In Vitro* $^1O_2$ Generation**

The intracellular $^1O_2$ generation was investigated using 2',7'-dichlorofluorescein diacetate (DCF-DA) as a fluorescent probe. Briefly, HeLa cells were first incubated with free Ce6, GCC, BMGCC or CMGCC ([Ce6] = 0.5 μg/mL) at physiological pH of 7.4 and tumor microenvironment pH of 6.5 for 2 h. The cells were then stained with DCF-DA (20 μM) for 20 min and washed with PBS 3 times. The prepared cells were irradiated with a 660 nm laser (100 mW/cm^2, 5 min) and observed with fluorescence microscopy (GFP channel).

Cellular Uptake and Intracellular Localization

The cellular uptake behavior was measured by CLSM and FACS. Briefly, HeLa cells were first incubated with free Ce6, GCC, BMGCC or CMGCC ([Ce6] = 0.5 μg/mL) at physiological pH of 7.4 and tumor microenvironment pH of 6.5 for 4 h. The culture medium was then removed by washing the cells with PBS 3 times. The confocal images and Ce6 fluorescent signals were then detected. To explore the intracellular distribution of the CMGCC, HeLa cells were incubated with CMGCC ([Ce6] = 2 μg/mL) at physiological pH of 7.4 for 4 h. The cell nuclei, mitochondria and lysosomes were stained with Hoechst, Mitotracker and Lysotracker, respectively, and observed under CLSM.

***In Vitro* MR Imaging**

HeLa cells were seeded in a 6-well plate at a density of 4 X 10^5 cells/well and incubated overnight. The medium was replaced by 2 mL of DMEM of pH 7.4 and 6.5 containing CMGCC at different Mn concentrations of 0, 6.25, 12.5 and 25 μM. After incubation for 4 h, the cells were washed with PBS for 3 times, trypsinized, centrifuged, and resuspended in 0.5 mL of agarose (0.5%) in 2 mL Eppendorf tubes before MR scanning. The pseudo-colored T_1-weighted MR images of the above agarose gel were captured on a 3.0 T MR imaging system (Ingenia 3.0T, Phillips, Netherlands) with the following parameters: TR = 600 ms, TE = 20 ms, NSA = 4.00, matrix = 152 × 247, slice gap = 0.5 mm, Voxel = 0.2 X 0.2 X 1 mm and FOV = 30 X 50 X 18 mm.

Animal Experiments

All animal experiments were performed according to the guidelines of the Institutional Animal Care and Use Committees (IACUC) of Donghua University and the policy of the National Ministry of Health. Female 3 to 4-week-old BALB/c nude mice (Shanghai Slac Laboratory Animal Center, Shanghai, China) were employed to establish a xenografted HeLa-tumor bearing mode using a method reported in our previous work.[1] The *in vivo* PDT was conducted when the tumor volume reached around 50 mm^3. Healthy ICR mice were employed to explore the *in vivo* pharmacokinetics and biodistribution behavior of the developed CMGCC.

Immunofluorescent Staining

The hypoxic condition of the tumor site was explored using an immunofluorescence staining assay. Briefly, HeLa tumor-bearing nude mice were i.v. injected *via* the tail vein with the developed GCC and CMGCC (200 μL, [Ce6] = 1.5 mg/kg). After 3 h, the tumors were excised 1.5 h after intraperitoneal injection of pimonidazole hydrochloride (0.6 mg per mouse). The collected tumor slices were first stained with mouse anti-pimonidazole monoclonal antibody, followed by staining with and Alex 488-conjugated goat anti-mouse secondary antibody for fluorescence imaging.

***In Vivo* Pharmacokinetics and Biodistribution**

To study the *in vivo* pharmacokinetics, healthy ICR mice (n = 3) were i.v. injected *via* the tail vein with the developed CMGCC (200 μL, [Ce6] = 1.5 mg/kg). The blood samples were collected at preset time points, digested in chloroazotic acid overnight, and analyzed by ICP-OES to quantify the Mn element. To explore the *in vivo* biodistribution behavior, CMGCC were i.v. injected in to HeLa tumor-bearing nude mice (n =3) and healthy ICR mice (n = 3) *via* tail vein (200 μL, [Ce6] = 1.5 mg/kg). The nude mice were sacrificed after 24 h. The ICR mice were sacrificed on day 1, 3 and 7. The major organs including the heart, liver, spleen, lungs, kidneys, brain and tumor were harvested, weighed, solubilized by chloroazotic acid overnight and then analyzed by ICP-OES to quantify Mn element.

Hemolysis Assay and Blood Routine Tests

A standard hemolysis assay was employed to study the hemocompatibility of the CMGCC nanoclusters according to our previous work.[2] Briefly, a blood sample (1.5 mL) was first diluted with PBS (3.5 mL), followed by centrifugation/redispersion process (2000 rpm, 10 min, 3 times) to give the red blood cells (RBCs). The achieved RBCs were diluted with 5 mL of PBS as stock. To conduct the hemolysis assay, 0.1 mL of the as-prepared RBCs was added to 0.9 mL of water (positive control), PBS (negative control) or CMGCC solutions with different concentrations (10, 25, 50, 100, and 200 μg/mL), respectively, and incubated at 37 ^{o}C for 2 h. Finally, all the above mixtures were centrifuged at 13000 rpm for 20 min, and the supernatant absorbance at 541 nm was recorded by UV-vis spectrometry. The hemolysis was determined by the equation: Hemolysis percentage (%) = $(A_{sample} - A_{negative\ control}) / (A_{positive\ control} - A_{negative\ control}) \times 100\%$.

For blood routine tests, healthy ICR mice were i.v. injected with the CMGCC (200 μL, [Ce6] = 1.5 mg/kg) or PBS as control. Blood samples were taken on day 7 and 14 post-injection (3 mice for each group) and analyzed by Mindray BC-2800vet Hematology Analyzer (Shenzhen Mindray Bio-Medical Electronics Co., Ltd., Shenzhen, China).

Table S1. Hydrodynamic size and polydispersity index (PDI) of all samples measured by DLS. CMGCC nanocluster formation was optimized with different feed ratio of 1:0.5, 1:1 and 1:2 (CM:GCC). BMGCC nanoclusters were obtained with a feed ratio of 1:1 (BM:GCC).

Samples	Hydrodynamic size (d. nm)	PDI
CM	34.4 ± 2.98 (peak)	0.17 ± 0.01
BM	28.4 ± 1.04 (peak)	0.14 ± 0.01
GCC	513.8 ± 14.8	0.27 ± 0.04
CMGCC (1:0.5)	245.1 ± 5.97	0.17 ± 0.04
CMGCC (1:1)	201.5 ± 2.32	0.22 ± 0.02
CMGCC (1:2)	234.0 ± 3.78	0.13 ± 0.02
BMGCC (1:1)	169.9 ± 6.23	0.21 ± 0.01

Table S2. Blood routine test results of healthy ICR mice i.v. injected with the CMGCC (200 μL, [Ce6] = 1.5 mg/kg). Blood samples were taken on day 7 and 14 post-injection. Mice treated with PBS were used as control. The blood routine tests include red blood cells (RBC), white blood cells (WBC), hemoglobin (HGB), hematocrit (HCT), mean corpuscular hemoglobin (MCH), mean corpuscular hemoglobin concentration (MCHC), mean corpuscular volume (MCV), platelet (PLT), and mean platelet volume (MPV). Reference ranges of hematology data for ICR mice were referred to Charles River Laboratories. Data are shown as mean ± SD (n = 3).

	RBC (M/μL)	**WBC (K/μL)**	**HGB (g/dL)**
Reference	8.78 ± 1.12	8.77 ± 2.95	14.55 ± 2.05
Control	9.21 ± 0.42	6.87 ± 1.26	15.53 ± 0.67
7 days	9.41 ± 0.58	7.68 ± 1.68	14.77 ± 0.89
14 days	9.34 ± 0.66	7.12 ± 1.53	15.28 ± 1.19
	HCT (%)	**MCH (pg)**	**MCHC (g/dL)**
Reference	49.43 ± 6.70	16.59 ± 1.09	29.52 ± 2.65
Control	53.40 ± 2.43	16.17 ± 0.25	29.10 ± 0.12
7 days	51.29 ± 2.88	17.08 ± 0.36	29.84 ± 0.37
14 days	52.78 ± 3.18	16.59 ± 0.78	29.45 ± 0.68
	MCV (fL)	**PLT (M/μL)**	**MPV (fL)**
Reference	56.39 ± 3.75	1383.53 ± 528.53	5.06 ± 0.44
Control	55.57 ± 0.78	1001.33 ± 72.57	5.31 ± 0.21
7 days	53.77 ± 1.27	1245.49 ± 62.28	5.14 ± 0.18
14 days	56.39 ± 1.63	1175.98 ± 95.57	5.23 ± 0.62

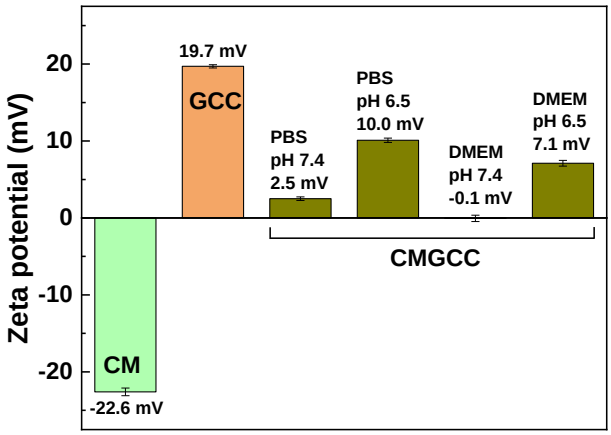

Figure S1. Zeta potential of CM nanoparticles (water), GCC micelles (water) and CMGCC nanoclusters (PBS, pH 7.4 and 6.5; DMEM containing 10% FBS, pH 7.4 and 6.5).

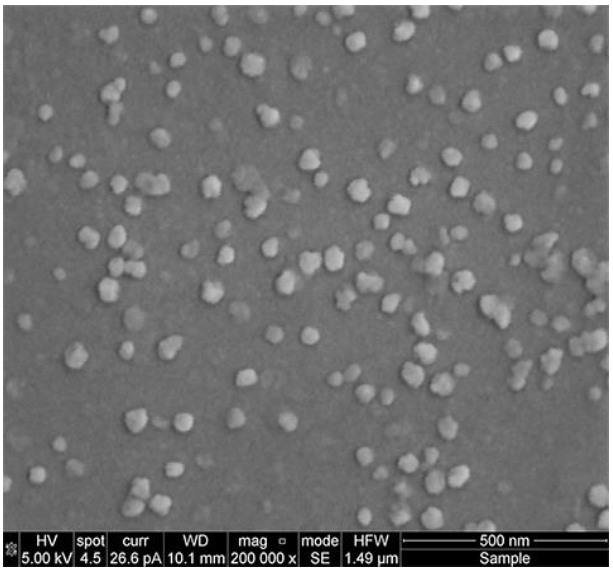

Figure S2. SEM image of CM nanoparticles.

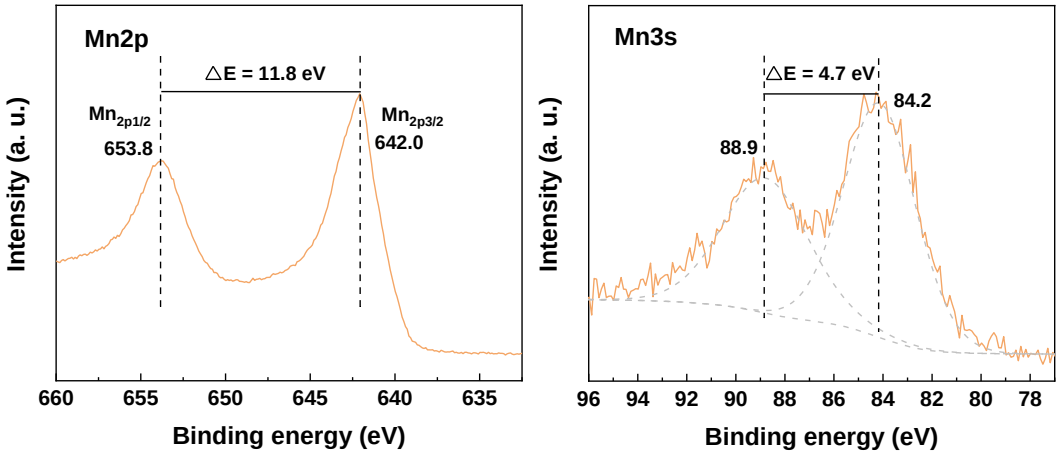

Figure S3. XPS spectra of Mn_{2p} and Mn_{3s} for CM nanoparticles. The peaks of $Mn_{2p3/2}$ and $Mn_{2p1/2}$ were recorded at the binding energy of around 642.0 and 653.8 eV, respectively. Two multiplet split peaks of Mn_{3s} were recorded at the binding energy of around 84.2 and 88.9 eV.

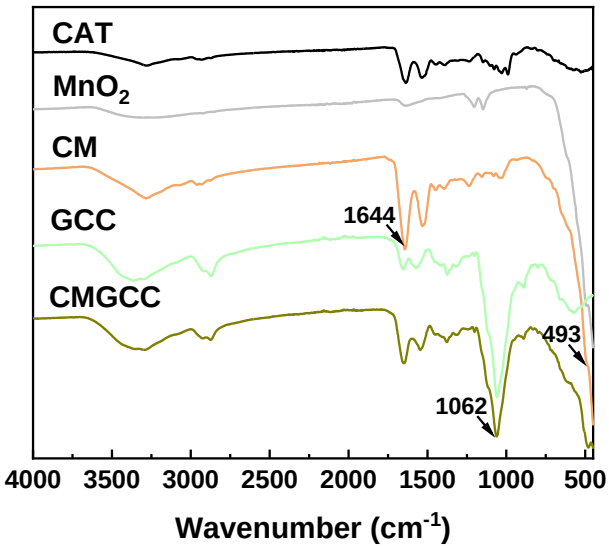

Figure S4. FTIR spectra of CAT, bare MnO_2, CM, GCC and CMGCC.

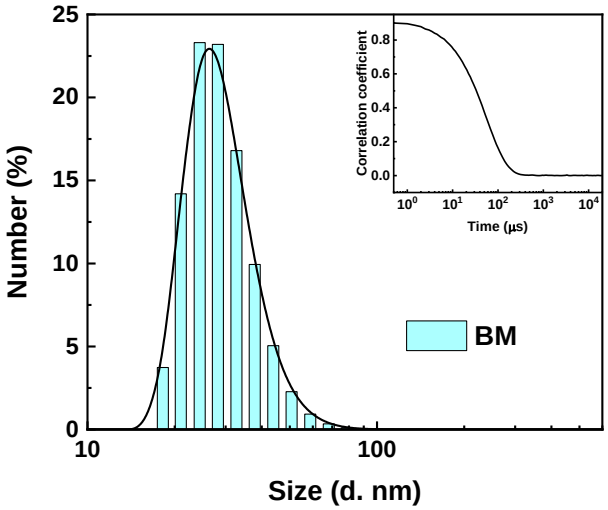

Figure S5. Hydrodynamic size distribution and correlation coefficient (inset) of BM nanoparticles in water.

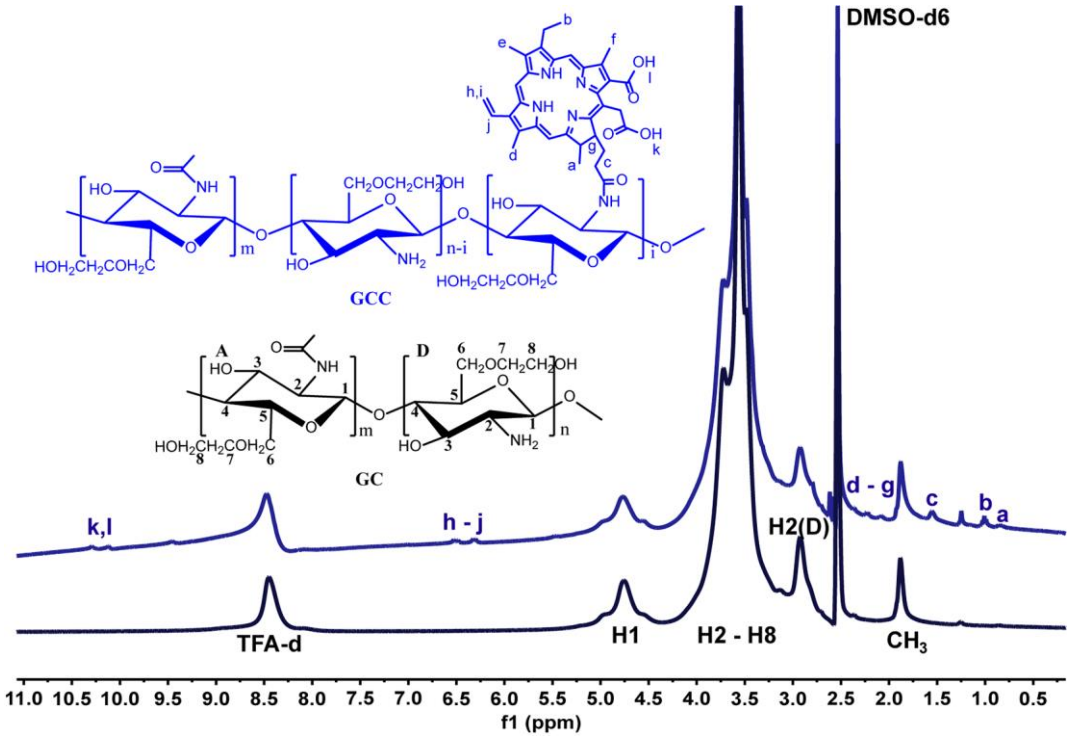

Figure S6. ^{1}HNMR spectra of glycol chitosan (GC) and the synthesized CE6 conjugated GC (GCC). Solvent: DMSO-d6 with a drop of TFA-d.

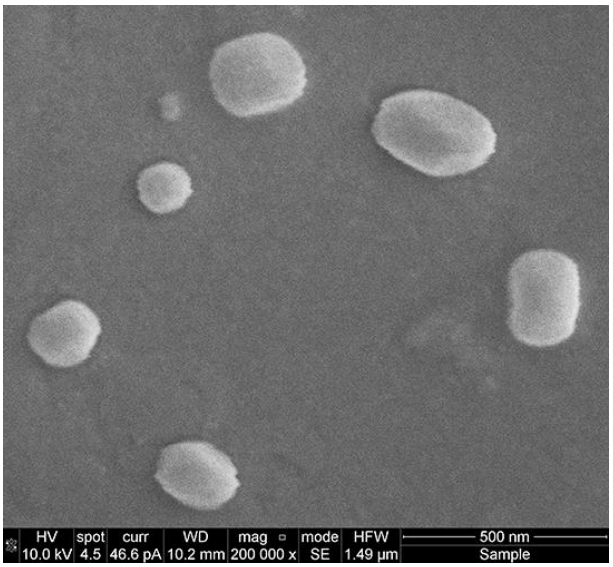

Figure S7. SEM image of GCC micelles.

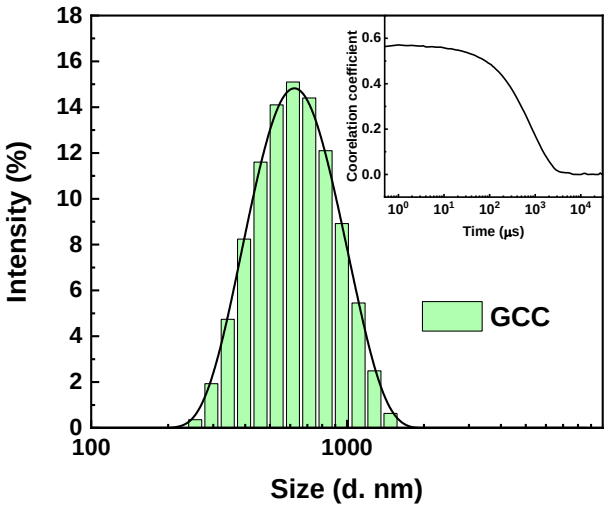

Figure S8. Hydrodynamic size distribution and correlation coefficient (inset) of GCC micelles in water.

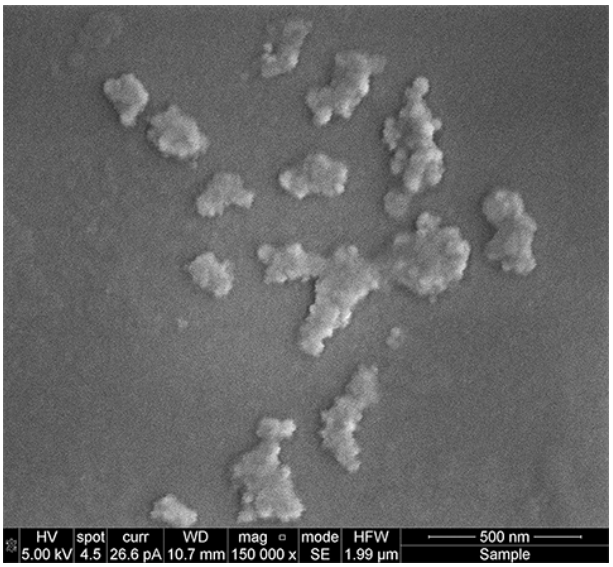

Figure S9. SEM image of CMGCC nanoclusters.

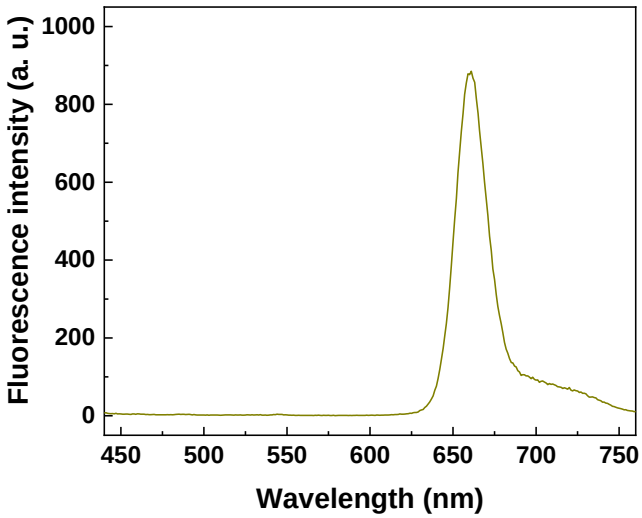

Figure S10. Fluorescence emission spectrum of CMGCC nanoclusters in water.

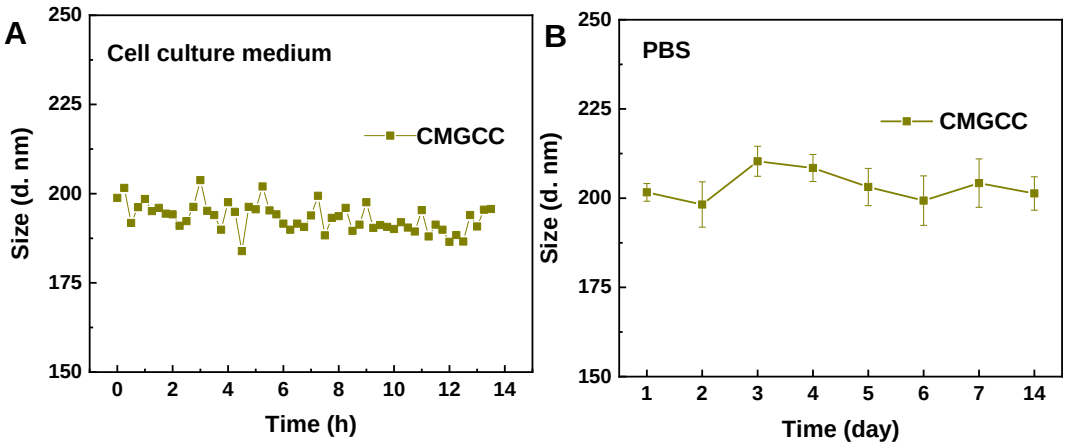

Figure S11. (A) Hydrodynamic size change of the developed CMGCC nanoclusters in cell culture medium (DMEM containing 10% of fetal bovine serum) throughout 14 h. (B) Hydrodynamic size change of the developed CMGCC nanoclusters in PBS over 14 days.

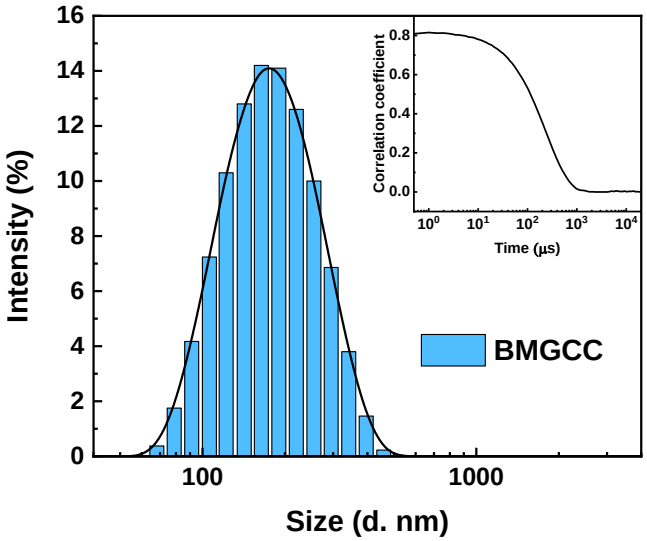

Figure S12. Hydrodynamic size distribution of BMGCC nanoclusters in water.

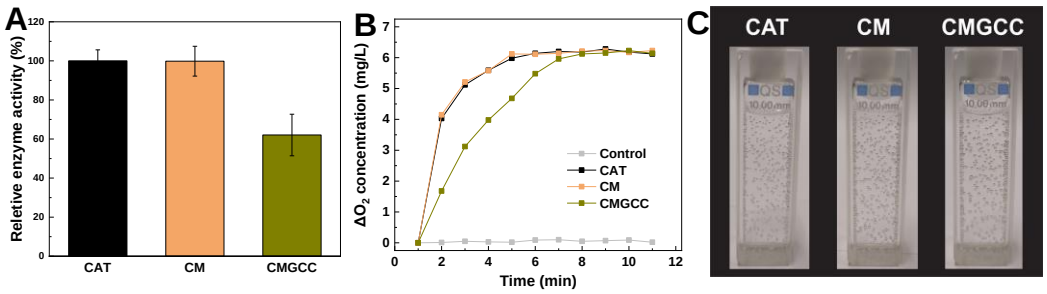

Figure S13. (A) Relative enzyme activity of native CAT, CM and CMGCC. (B) Oxygen concentration in H_2O_2 solutions (500 μM) incubated with CAT, CM and CMGCC. (C) Photographs of O_2 bubble generation in H_2O_2 solutions incubated with CAT, CM and CMGCC.

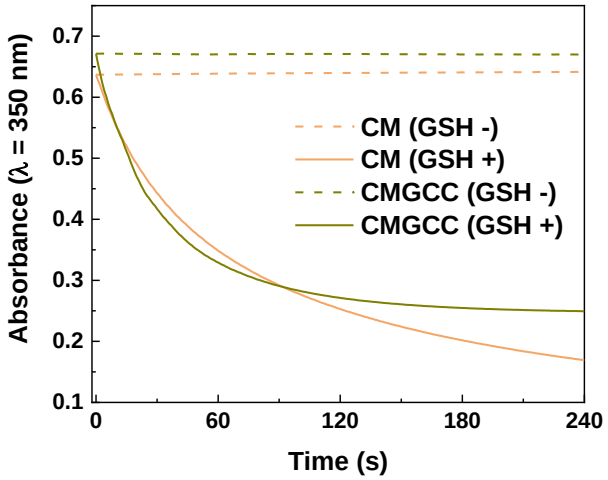

Figure S14. UV-vis absorbance change (λ = 350 nm) of MnO_2 in CM and CMGCC in the presence or absence of GSH (10 mM).

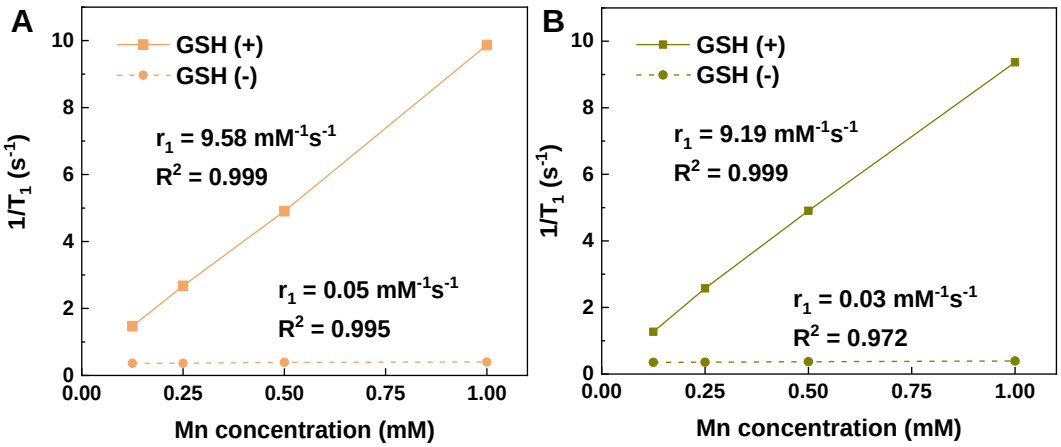

Figure S15. Linear fitting of $1/T_1$ of CM (A) and CMGCC (B) as a function of Mn concentration in the presence and absence of GSH (10 mM).

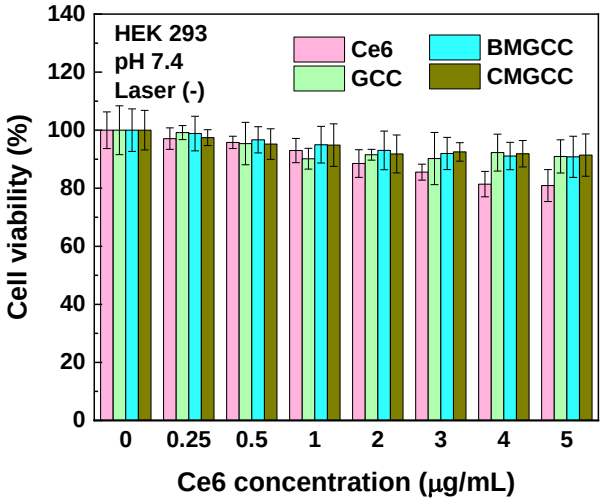

Figure S16. Cell viabilities of HEK 293 cells treated with Ce6, GCC and BMGCC and CMGCC at different Ce6 concentrations under pH 7.4 in the absence of laser irradiation.

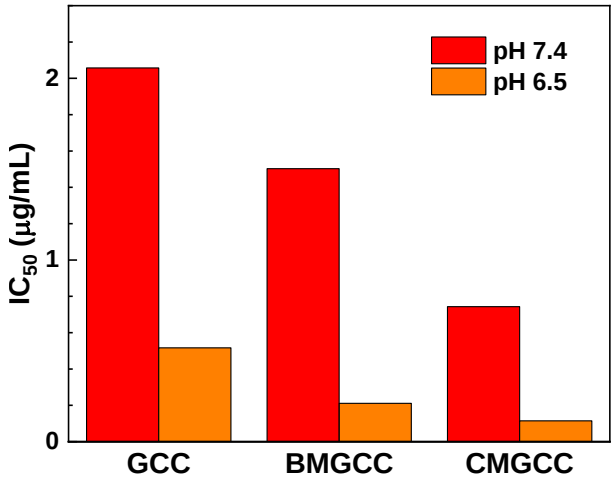

Figure S17. IC_{50} values of GCC, BMGCC and CMGCC toward HeLa cells at pH 7.4 and 6.5. GCC: 2.06 μg/mL (pH 7.4), 0.52 μg/mL (pH 6.5); BMGCC: 1.50 μg/mL (pH 7.4), 0.21 μg/mL (pH 6.5); CMGCC: 0.74 μg/mL (pH 7.4), 0.12 μg/mL (pH 6.5) .

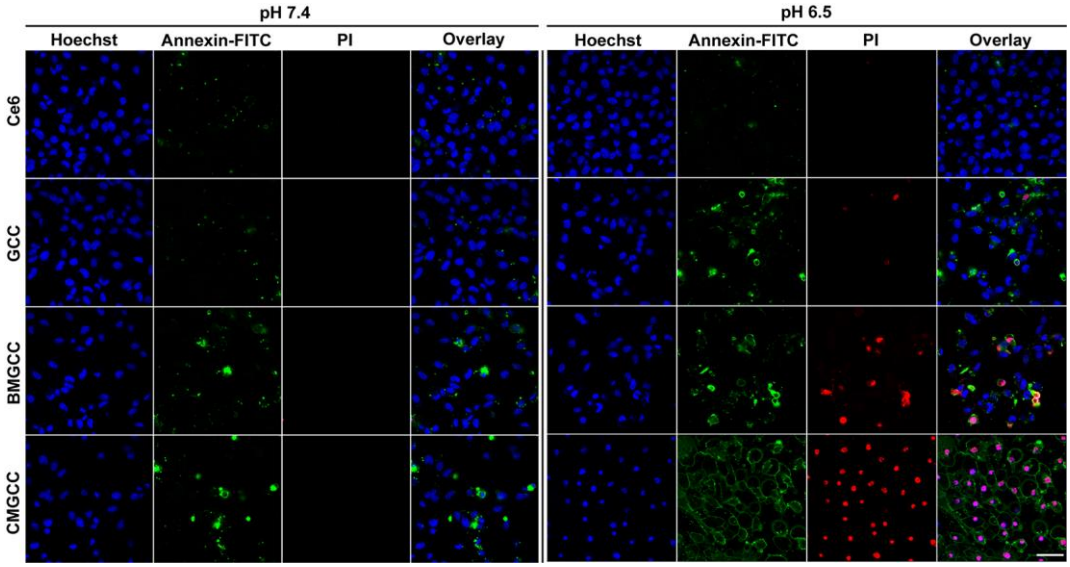

Figure S18. CLSM images of HeLa cells after treatment with Ce6, GCC, BMGCC and CMGCC ([Ce6] = 0.5 μg/mL) with 660 nm laser irradiation (100 mW/cm^2, 5 min) at pH 7.4 and 6.5. The cell nuclei, early apoptotic and dead cells were stained with Hoechst, FITC-Annexin V and PI, respectively. Scale bar = 50 μm.

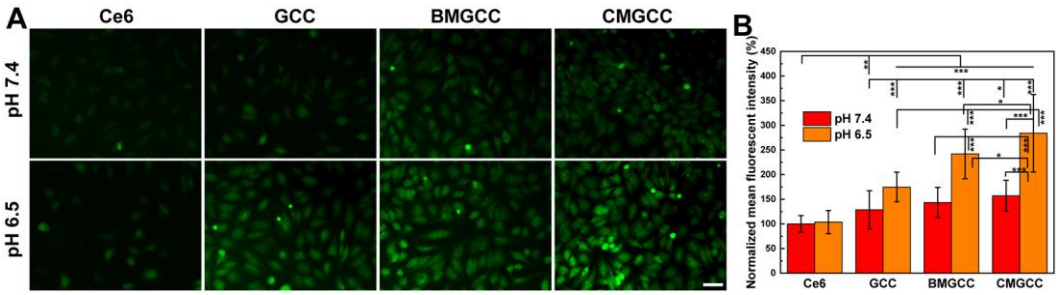

Figure S19. (A) Intracellular $^1O_2$ generation in HeLa cells after treatment with Ce6, GCC, BMGCC and CMGCC ([Ce6] = 0.5 μg/mL) with 660 nm laser irradiation (100 mW/cm^2, 5 min) at pH 7.4 and 6.5 using the DCF-DA fluorescent probe. Scale bar = 50 μm. (B) Normalized mean fluorescence intensity of HeLa cells after different tratments. The mean fluorescence intensity was determined using Image J software with counting 20 cells randomly selected from the fluorescent images.

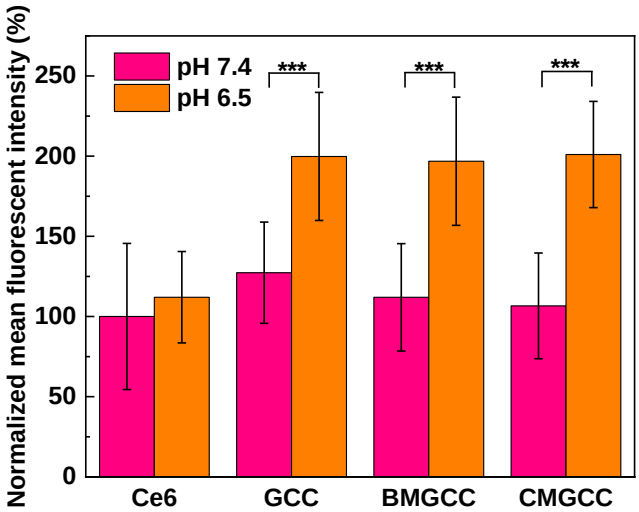

Figure S20. Normalized mean Ce6 fluorescence intensity of HeLa cells after treatment with Ce6, GCC, BMGCC and CMGCC ([Ce6] = 0.5 μg/mL) at pH 7.4 and 6.5. The mean fluorescence intensity was determined using Image J software with counting 20 cells randomly selected from the CLSM images.

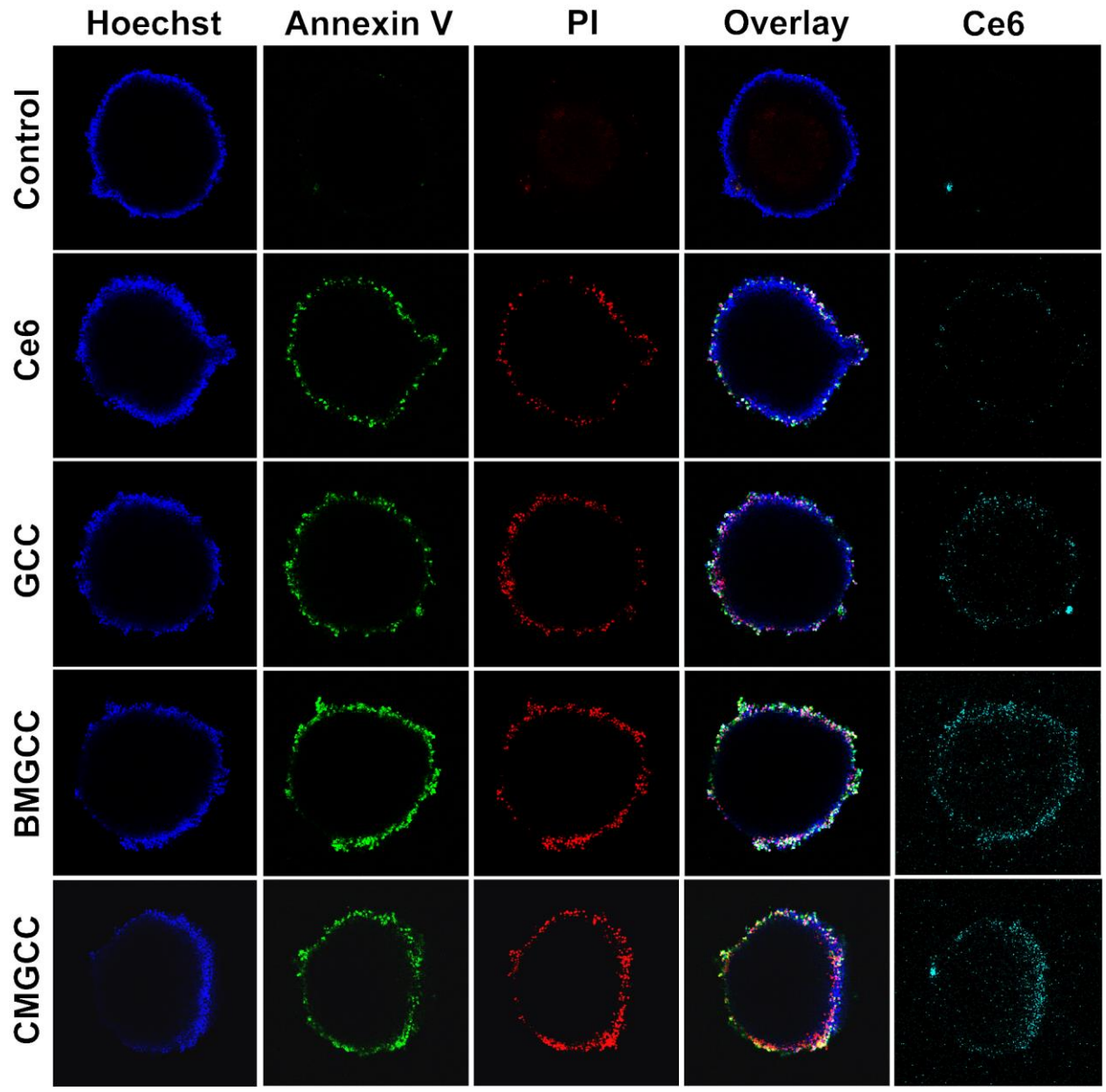

Figure S21. CLSM images of 3D MCSs after treatment with Ce6, GCC, BMGCC and CMGCC ([Ce6] = 0.5 μg/mL) with 660 nm laser irradiation (100 mW/cm^2, 5 min) at pH 7.4. The cell nuclei, early apoptotic and dead cells were stained with Hoechst, FITC-Annexin V and PI, respectively.

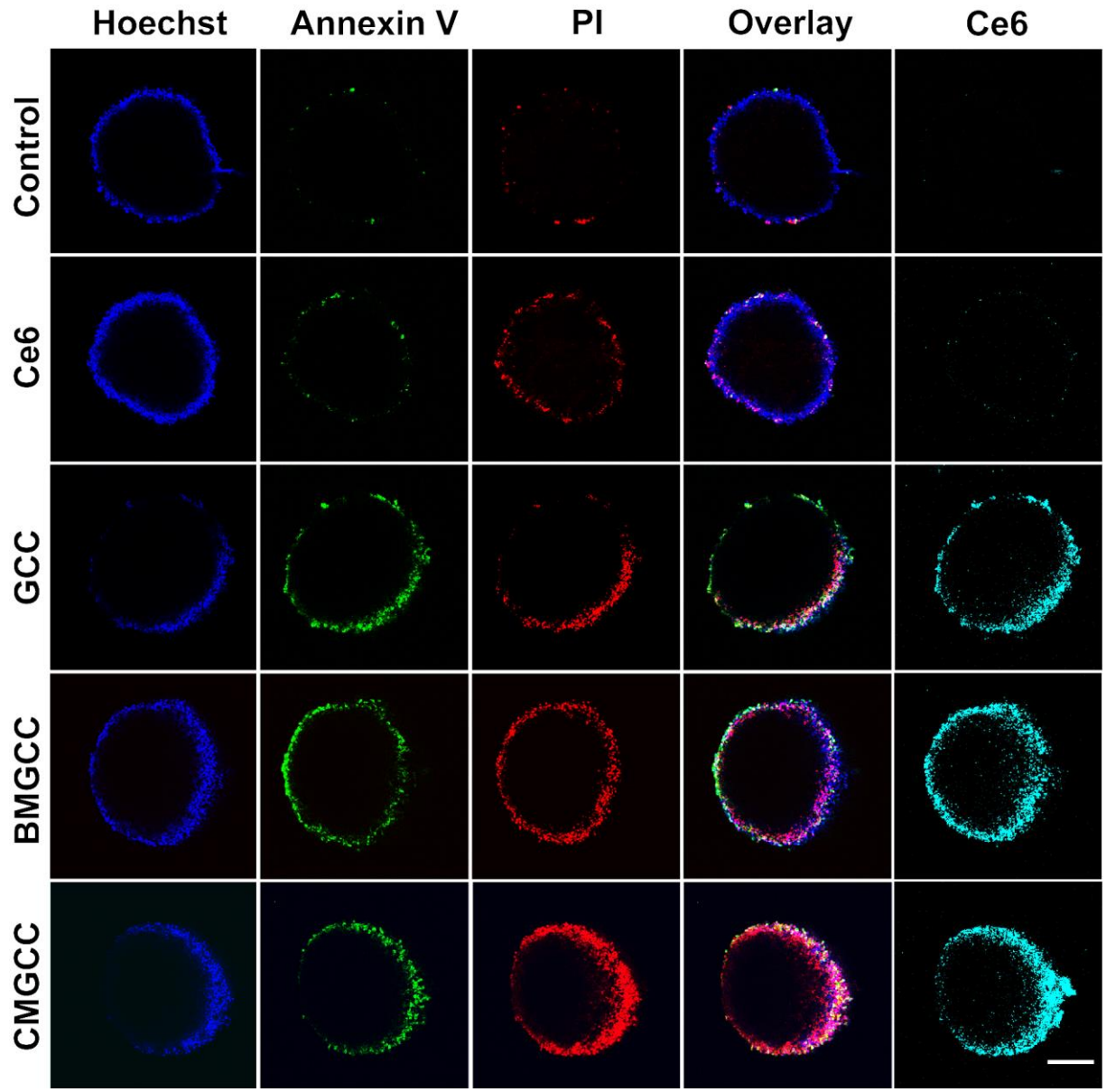

Figure S22. CLSM images of 3D MCSs after treatment with Ce6, GCC, BMGCC and CMGCC ([Ce6] = 0.5 μg/mL) with 660 nm laser irradiation (100 mW/cm^2, 5 min) at pH 6.5. The cell nuclei, early apoptotic and dead cells were stained with Hoechst, FITC-Annexin V and PI, respectively.

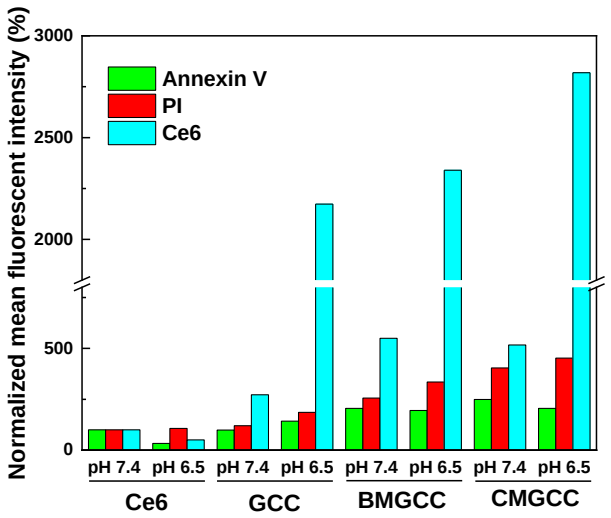

Figure S23. Normalized fluorescence intensity of 3D MCSs after treatment with Ce6, GCC, BMGCC and CMGCC ([Ce6] = 0.5 μg/mL) with 660 nm laser irradiation (100 mW/cm^2, 5 min) at pH 7.4 and 6.5. The mean fluorescence intensity was determined using Image J software.

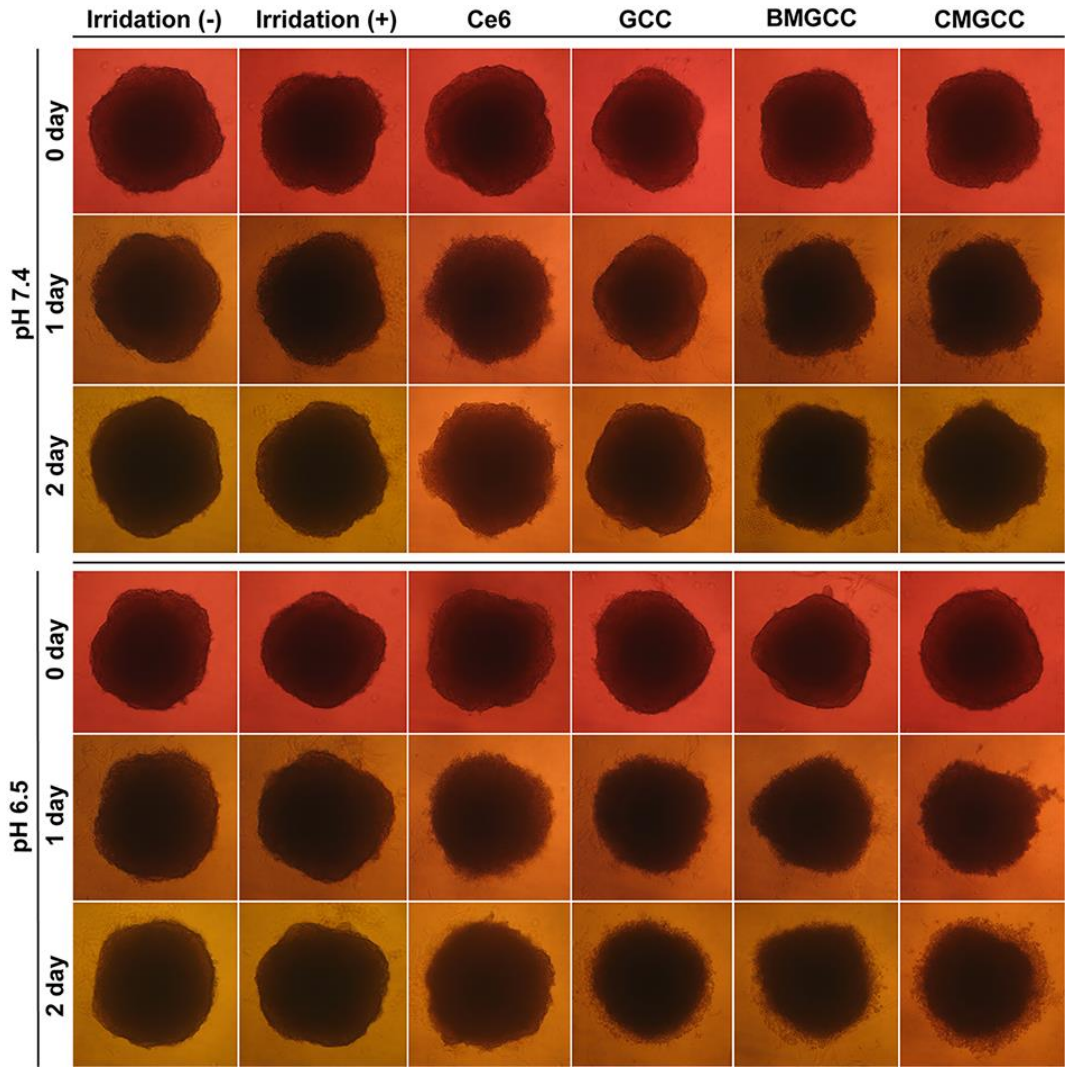

Figure S24. Optical images of 3D MCSs over time after treatment with Ce6, GCC, BMGCC and CMGCC ([Ce6] = 5 μg/mL) with 660 nm laser irradiation (100 mW/cm^2, 5 min) at pH 7.4 and 6.5. The diameter of the MCSs is 500 – 800 μm.

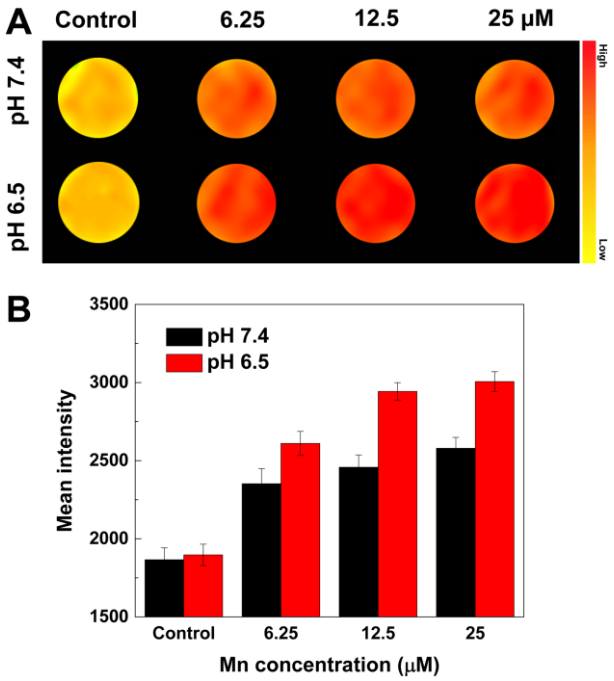

Figure S25. (A) T_1-weighted MR images and (B) relative mean intensity analysis of HeLa cells treated with CMGCC at Mn concentrations of 0, 6.25, 12.5 and 25 μM for 4 h. The color bar from yellow to red indicates the gradual increase of MR signal intensity.

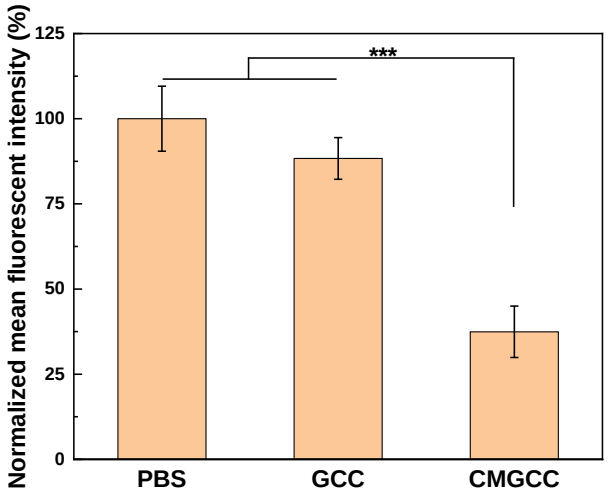

Figure S26. Normalized mean antipimonidazole antibody fluorescence intensity of tumor slices after different treatments. The mean fluorescence intensity was determined using Image J software with counting the 5 dashed rectangle in each image.

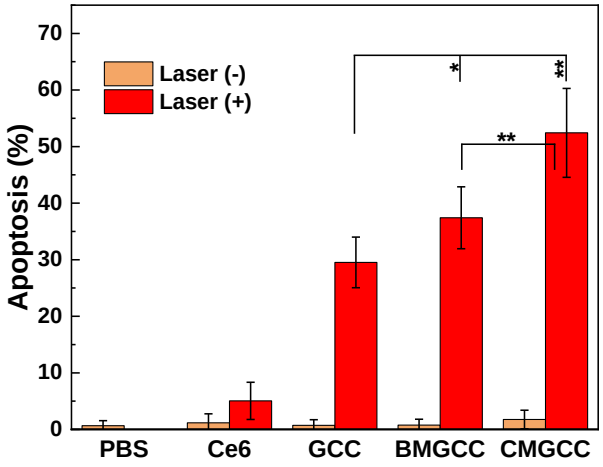

Figure S27. Quantitative analysis of the apoptosis rate of tumor cells after different treatments. The ratio was determined by counting the normal cells and necrotic/apoptotic cells in the 5 dashed rectangles in each image of Fig 5F. PBS: 0.66% (laser -), 0% (laser +); Ce6: 1.16% (laser -), 5.05% (laser +); GCC: 0.72% (laser -, 29.52% (laser +); BMGCC: 0.76% (laser -), 37.42% (laser +); CMGCC: 1.75% (laser -), 54.43% (laser +).

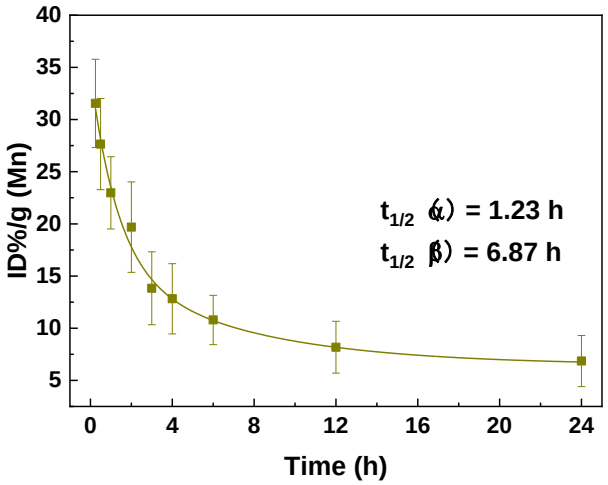

Figure S28. Blood circulation curve of CMGCC in healthy ICR mice by tracking the Mn concentration in blood at different time intervals after i.v. injection *via* tail vein ([MnO_2] = 4.2 mg/kg).

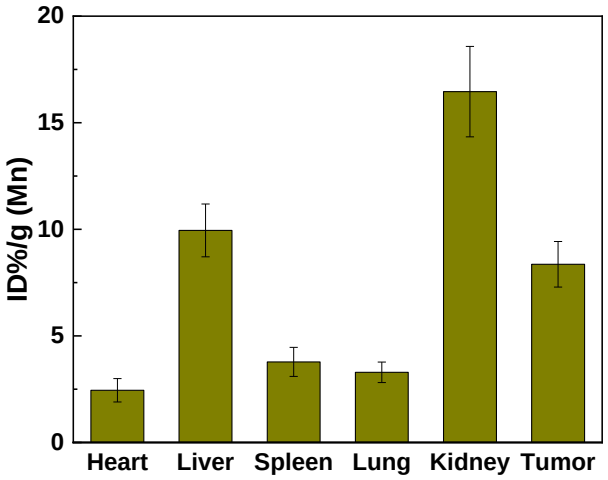

Figure S29. *In vivo* biodistribution of CMGCC in HeLa tumor-bearing nude mice at 24 h post-injection ([MnO_2] = 4.2 mg/kg).

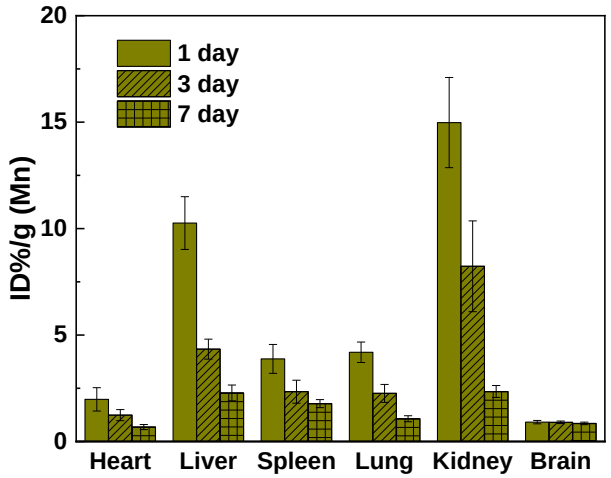

Figure S30. *In vivo* biodistribution of CMGCC in healthy ICR mice on day 1, 3 and 7 after i.v. injection *via* tail vein ([MnO_2] = 4.2 mg/kg).

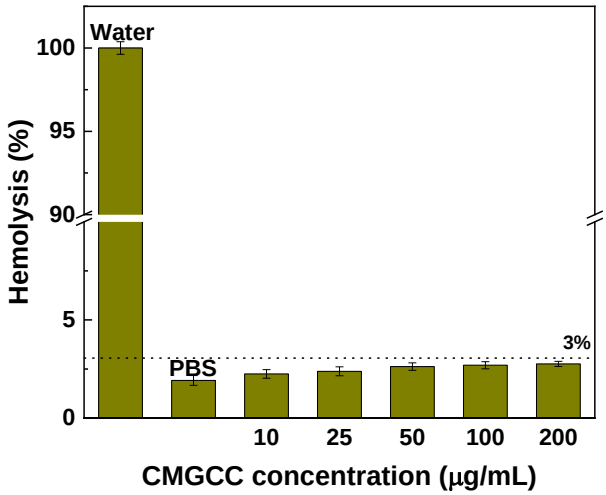

Figure S31. Hemolysis induced by CMGCC at various concentrations. RBCs incubated with water and PBS were used as the positive and negative control, respectively.

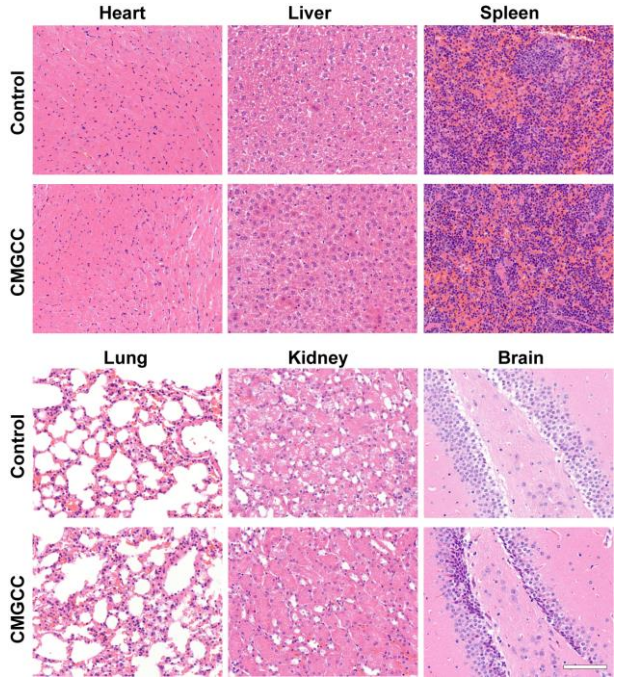

Figure S32. H&E staining of heart, liver, spleen, lung, kidney and brain from nude mice on day 21 post-injection of the CMGCC. Mice without any treatment were used as control. Scale bar = 100 μm.

References

1. Zhu, J.; Peng, C.; Sun, W.; Yu, Z.; Zhou, B.; Li, D.; Luo, Y.; Ding, L.; Shen, M.; Shi, X., Formation of Iron Oxide Nanoparticle-Loaded γ-Polyglutamic Acid Nanogels for MR Imaging of Tumors. *J. Mater. Chem. B* **2015,** *3*, 8684-8693.

2. Xu, F.; Zhu, J.; Lin, L.; Zhang, C.; Sun, W.; Fan, Y.; Yin, F.; van Hest, J. C. M.; Wang, H.; Du, L.; Shi, X., Multifunctional PVCL Nanogels with Redox-Responsiveness Enable Enhanced MR Imaging and Ultrasound-Promoted Tumor Chemotherapy. *Theranostics* **2020,** *10*, 4349-4358.